JVSTB Journal of Vacuum Science & Technology B

Quantitative dopant profiling of p - n junction in In Ga As ∕ Al Ga As light-emitting diode using off-axis electron holography

Suk Chung, Shane R. Johnson, Ding Ding, Yong-Hang Zhang, David J. Smith, and Martha R. McCartney

Citation: Journal of Vacuum Science & Technology B **28**, C1D11 (2010); doi: 10.1116/1.3244575
View online: http://dx.doi.org/10.1116/1.3244575
View Table of Contents: http://scitation.aip.org/content/avs/journal/jvstb/28/1?ver=pdfcov
Published by the AVS: Science & Technology of Materials, Interfaces, and Processing

Quantitative dopant profiling of *p-n* junction in InGaAs/AlGaAs light-emitting diode using off-axis electron holography

Suk Chung[a)]
School of Materials, Arizona State University, Tempe, Arizona 85287

Shane R. Johnson, Ding Ding, and Yong-Hang Zhang
Center for Nanophotonics, Arizona State University, Tempe, Arizona 85287 and Department of Electrical Engineering, Arizona State University, Tempe, Arizona 85287

David J. Smith and Martha R. McCartney[b)]
Department of Physics, Arizona State University, Tempe, Arizona 85287

(Received 16 June 2009; accepted 14 September 2009; published 3 March 2010)

The electrostatic potential profile across the *p-n* junction of an InGaAs light-emitting diode with linearly graded AlGaAs triangular barriers has been measured using off-axis electron holography. Simulations of the junction profile show small discrepancies with experimental measurements in the region of the *p*-and *n*-doped AlGaAs barriers, which are located away from the InGaAs quantum wells. Revised simulations reproduce the measurements reasonably when a carrier-trap density of 6×10^{16} cm^{-3} in the AlGaAs barriers is subtracted from the dopant concentrations. The presence of oxygen impurities is considered as the most likely reason for the reduction in doping efficiency.
 [DOI: 10.1116/1.3244575]

I. INTRODUCTION

AlGaAs/GaAs heterostructures have received much attention in recent years due to their novel properties which make them suitable for optoelectronic applications, including laser diodes, light-emitting diodes (LEDs), and high electron mobility transistors.[1,2] $Al_xGa_{1-x}As/GaAs/Al_xGa_{1-x}As$ quantum wells (QWs) with triangular AlGaAs barriers have been extensively investigated, with the objective being to improve the carrier transport properties through the use of the linearly graded barriers.[3,4] However, unintentional impurities located in the AlGaAs barrier layers have been reported to degrade the expected performance of devices based on AlGaAs/GaAs heterostructures.[5,6] Studies to determine the nature of these impurities have been conducted using a range of techniques including deep-level transient spectroscopy,[5,7] secondary-ion mass spectroscopy,[8] and photoluminescence measurements.[5] According to these studies, it has been found that the photoluminescence intensity is inversely proportional to the concentration of deep-level electron traps.[5] The threshold current of optical devices is also closely related to the concentration of oxygen impurities.[6]

Dopant distribution and activation are critical to device performance, since these parameters determine the electrostatic potential distributions within real devices. However, as the dimensions of semiconductor devices decrease, direct experimental determination of the potential profile represents a demanding challenge. Off-axis electron holography with the electron microscope is an interferometric technique which allows convenient access to both amplitude and phase information. Since the phase shift of the electron wavefunction depends on the local electric field distributions within the sample, the electron holography technique can be used to provide quantitative information about electrostatic potential variations in materials, with nanometer-scale resolution.[9] Off-axis electron holography has been widely used to measure potential profiles associated with dopant distributions in, for example, Si *p-n* junctions,[10,11] and Si transistors,[12,13] including one device having a 30 nm gate length.[14] The potential distributions present within compound semiconductor devices are also of considerable interest, but only a very limited number of experimental holography studies have so far been reported.[15,16] Moreover, very little attention has been given to studying compound semiconductors which have varying alloy compositions that cause variations in the mean inner potential (MIP) of the material, which in turn complicate hologram interpretation.

In this article, off-axis electron holography has been used to measure the electrostatic potential profile across an $In_{0.2}Ga_{0.8}As$ LED *p-n* junction which has linearly graded $Al_xGa_{1-x}As$ barriers, where the concentrations of the Si and Be dopants were also exponentially varied. A careful comparison between the experimental and simulated *p-n* junction potential ($V_{p\text{-}n}$) distributions allowed the density of carrier traps in the AlGaAs layers to be determined.

II. EXPERIMENTAL DETAILS

The samples were grown by molecular beam epitaxy (MBE) in a VG V80H solid-source system, and the sample cross section is schematically illustrated in Fig. 1. The epilayers were grown on a semi-insulating GaAs (100) substrate and consisted of (I) 1280-nm-thick Si-doped (*n*-type) GaAs contact layer, (II) 210-nm-thick Si-doped (*n*-type) $Al_xGa_{1-x}As$ barrier layer where the Al mole fraction (x) was linearly graded from 0.05 up to 0.20 and back down to 0.05, (III) 170-nm-thick undoped active region containing three

a)Electronic mail: suk.chung@asu.edu
b)Electronic mail: molly.mccartney@asu.edu

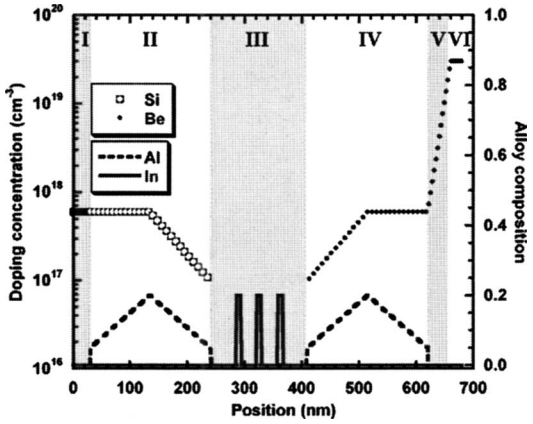

FIG. 1. Schematic of InGaAs LED sample structure showing Al and In compositions and nominal Si and Be concentrations. Growth direction is from left to right. Region I: Si-doped *n*-GaAs contact; region II: Si-doped $Al_xGa_{1-x}As$ barrier; region III: undoped triple $In_{0.2}Ga_{0.8}As$/GaAs QWs; region IV: Be-doped $Al_xGa_{1-x}As$ barrier; region V: Be-doped GaAs; region VI: Be-doped *p*-GaAs contact. Only the part of region I is shown in schematic.

7-nm-thick $In_{0.2}Ga_{0.8}As$ QWs embedded in GaAs, (IV) 210-nm-thick Be-doped (*p*-type) $Al_xGa_{1-x}As$ barrier layer where the Al mole fraction was linearly graded from 0.05 up to 0.20 and back down to 0.05, (V) 40-nm-thick Be-doped (*p*-type) GaAs layer, and (VI) 20-nm-thick Be-doped (p^+) GaAs contact layer. This electron holography study focuses on the $V_{p\text{-}n}$ profile across regions I–V.

Samples suitable for observation by scanning transmission electron microscopy (STEM) and off-axis electron holography were prepared using a Multiprep™ wedge-polishing apparatus using a wedge angle of 2°. The holography samples were mechanically polished *without* ion milling down to thicknesses, which overlap the optimum range needed for holography analysis.[17,18] This thinning procedure is critical for minimizing the possibility of an electrically inactive layer that might otherwise result from extensive ion milling.[19,20] The optimum thickness range results from a trade-off between the need for a strong phase signal against the increasing background noise caused by increases in inelastic scattering with greater sample thickness.[21] A thinner sample area is necessary for STEM imaging and analysis. Thus, Ar-ion milling was used for a few minutes at 3.5 keV, with a current of 13 μA and a milling angle of 5°.

Off-axis electron holograms were recorded using a Philips CM200 field-emission gun TEM operated at 200 keV, as reported elsewhere.[22] In the Lorentz imaging mode, a biprism voltage of ~110 V was used, giving rise to interference fringes with a contrast of ~40% and a spacing of 3.8 nm. An effective pixel size of 6 nm was obtained in the reconstructed phase image for a magnification of 20 k× at the charge coupled device camera, and lateral averaging of experimental profiles over ten adjacent pixels gave significant improvement in the nominal sensitivity.[9] During the holography observations, the samples were tilted by ~5° away from the [110] zone axis about the substrate normal in order to minimize dynamical diffraction effects,[23] and reference holograms were used to correct for any nonlinearities in the imaging and recording system.[24] *Z*-contrast STEM images were recorded using a JEM2010F TEM equipped with an annular-dark-field (ADF) detector.

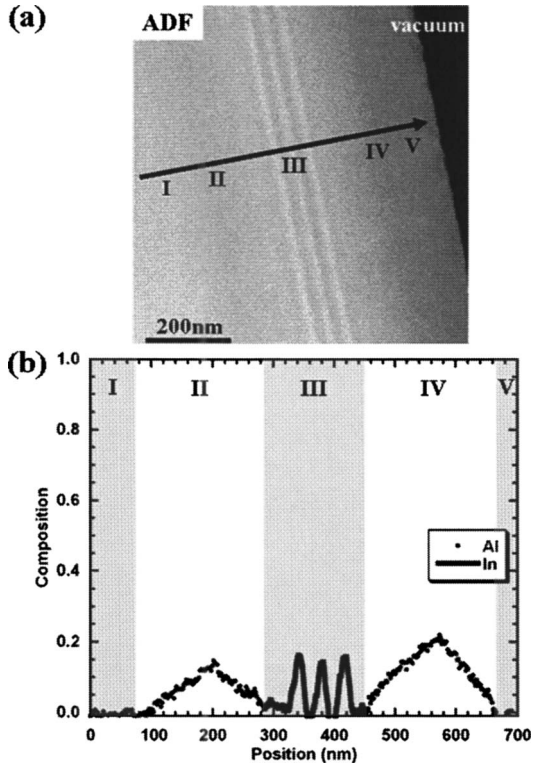

FIG. 2. (a) Annular-dark-field STEM cross-sectional image of InGaAs LED showing barriers and active layers. Note that the bands of darker contrast correspond to the $Al_xGa_{1-x}As$ barrier layers in regions II and IV, and lines of brighter contrast correspond to the three InGaAs QWs in region III. (b) Corresponding composition profiles, from the line indicated in (a), which confirm Al and In concentrations across entire layer sequence.

III. RESULTS AND DISCUSSION

A typical cross section of the InGaAs LED sample, recorded in the ADF STEM imaging mode, is shown in Fig. 2(a). In this *Z*-contrast imaging mode, the image intensity (I) is proportional to the atomic number (Z) of the specimen, as given by the expression $I \sim Z^{\alpha}$, where the constant α has the value of 1.7 in these experiments.[25] Thus, the three InGaAs QWs in the GaAs active layer (region III) are clearly visible as the lines of brighter contrast. Moreover, the bands of darker contrast correspond to the graded AlGaAs barriers (regions II and IV) which have Al mole fractions that are as large as 0.2. Figure 2(b) shows the corresponding composition profiles for the line indicated in (a), which are calculated based on the measured *Z*-contrast intensities. Overall, the profiles confirm the Al and In compositions across the entire sequence of layers, which compare well with nominal values when uncertainties in alloy compositions and experimental measurements are considered. The top GaAs layer has darker contrast than the GaAs buffer layer because of thickness curvature at the front edge of the sample due to ion milling. This thickness variation was taken into account when calculating elemental compositions.

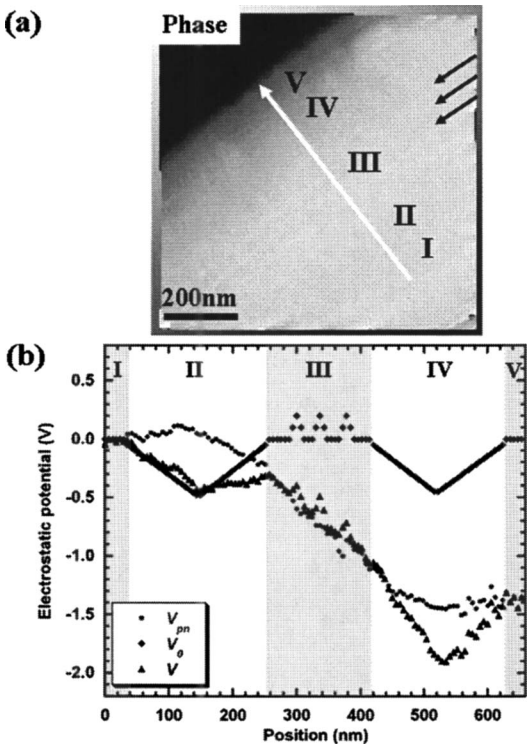

FIG. 3. (a) Reconstructed holographic phase image of InGaAs LED. The black arrows indicate positions of three InGaAs QWs. (b) Electrostatic potential profiles V, $V_{p\text{-}n}$, and V_0, from the line indicated in (a), where $V_{p\text{-}n}$ was extracted by subtracting V_0 from V.

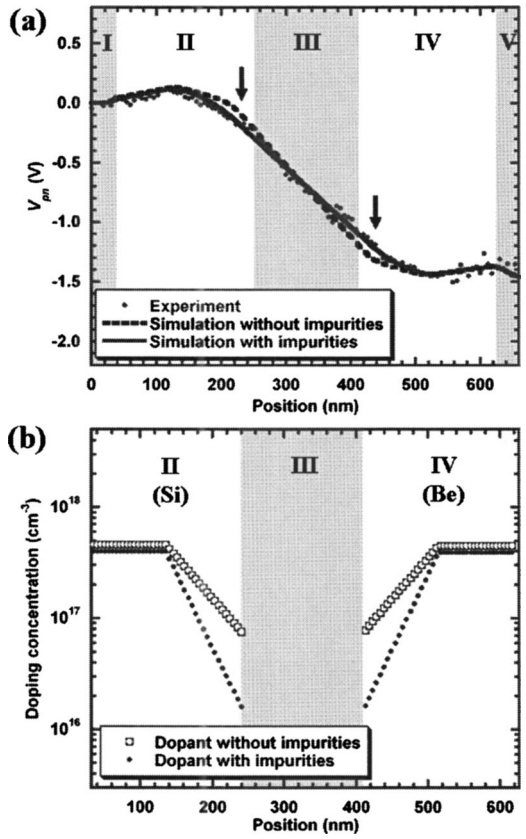

FIG. 4. (a) InGaAs LED $V_{p\text{-}n}$ profile comparisons between experiment and simulations with and without carrier traps in AlGaAs barriers. The arrows indicate regions of discrepancy between measurement and simulation without impurities. (b) Concentration profiles of donors (region II) and acceptors (region IV) with and without carrier traps in AlGaAs barriers.

Figure 3(a) shows a reconstructed holographic phase image of the InGaAs LED. The sample thickness in the analyzed area was estimated using the ratio between the amplitude of the reference hologram and the reduced amplitude caused by inelastic scattering.[26] Using this relationship, the sample thicknesses within the analyzed area were determined to range from 100 to 200 nm. The values used for the inelastic mean free path in the calculations are the published values of 67 nm for GaAs and 77 nm for AlAs,[18] a linear interpolation of these two values for the $Al_xGa_{1-x}As$ layers, and a value of 62 nm for $In_{0.2}Ga_{0.8}As$ which was determined by fitting to the experimental measurements.

The electrostatic potential profile was then extracted from the thickness and phase information using the expression:[27]

$$\phi = \frac{2\pi e}{\lambda E} \times \frac{E_0 + E}{2E_0 + E} Vt = C_E Vt = C_E(V_0 + V_{p\text{-}n})t, \qquad (1)$$

where e and λ are the charge and wavelength of the incident electron, t is the sample thickness, E is the electron kinetic energy, E_0 is the electron rest energy, C_E is an energy-related constant (0.007 28 rad V^{-1} nm^{-1} for 200 keV electrons), V is the electrostatic potential, and V_0 is the MIP. The electrostatic potential profile labeled V is shown in Fig. 3(b) for the line profile indicated in Fig. 3(a). The measured phase shift results not only from the dopant distribution across the *p-n* junction but also from the variation in V_0. Thus, its contribution to the electrostatic potential must be subtracted in order to determine $V_{p\text{-}n}$. The V_0 profile in the AlGaAs layers was calculated using the published MIP values for GaAs and AlAs,[18] and assuming that the MIP varied linearly with Al mole fraction. Furthermore, the MIP difference of 0.2 V between the $In_{0.2}Ga_{0.8}As$ and GaAs layers was utilized in the calculation, which was determined by fitting to the measurement. Linearly graded MIP differences were used at the InGaAs/GaAs interfaces rather than abrupt values because the phase images of the interfaces were not ideally sharp due to insufficient sampling of holography measurements. The result is also shown in Fig. 3(b), together with $V_{p\text{-}n}$.

The $V_{p\text{-}n}$ profile was simulated using a one-dimensional Poisson solver[28] and with the published doping efficiency values of 83% (A_{Si}) for Si-doped $Al_{0.10}Ga_{0.90}As$,[29] and 75% (A_{Be}) for Be-doped $Al_{0.65}Ga_{0.35}As$.[30] The experimental measurements provide the electrostatic potential profile within an arbitrary voltage offset, which was chosen so that both the measured and simulated $V_{p\text{-}n}$ profiles were zero in the GaAs contact layer (region I). By comparing the experimental and simulated profiles in Fig. 4(a), it becomes apparent that the experimental $V_{p\text{-}n}$ profile in the *n*- and *p*-doped AlGaAs barriers near the GaAs active layer shows some discrepancy with the simulation, as indicated by the arrows.

The absolute accuracy of these measurements has been improved by lateral averaging of the potential profiles to approximately 0.03 V, which is close to the maximum discrepancy between the experimental and simulated profiles.

However, the shape and, most importantly, the slope of $V_{p\text{-}n}$ near and throughout the active region of this *p-n* junction structure (which is depleted) is very sensitive to the doping profile of the graded AlGaAs barriers on either side. Thus, it is clear that the experimental holography results predict a much reduced doping level in the graded AlGaAs barriers near the barrier/active region interface than the nominal expected dopant levels that were based on prior calibrations of Si- and Be-doped GaAs.

In order to improve the agreement with experiment, the simulations were revised to include a reduction in doping efficiency caused by carrier traps that could result from unintentional oxygen impurities in the AlGaAs layers. This effect can be described using the approximate expression:

$$n = A \times N_{\text{nom}} - N_{\text{trap}}, \tag{2}$$

where n is the carrier concentration, A is the efficiency of dopant activation, N_{nom} is the nominal doping impurity concentration (Si or Be), and N_{trap} is the carrier-trap density. The electrostatic potentials for the experimental measurements and simulations with and without carrier traps are compared in Fig. 4(a). The potential simulation using N_{trap} densities of $(6 \pm 1) \times 10^{16}$ cm^{-3} agrees reasonably with experiment, especially in the *p*- and *n*-doped AlGaAs regions. The dopant profiles with and without the presence of carrier traps are compared in Fig. 4(b), showing that the effect of these traps on doping efficiency becomes dominant as dopant concentrations decrease near the barrier/active region interface.

Finally, it can be asserted, although not proven here, that these results are consistent with reports in the literature where it has been found that unintentional oxygen impurities in AlGaAs layers grown by MBE act as deep-level nonradiative centers,[5,6] with typical concentrations ranging from 1×10^{16} to 1×10^{18} cm^{-3} depending on growth conditions.[6,8] It has also been reported that the typical carrier-trap densities range from 1×10^{15} to 1×10^{17} cm^{-3} depending on Al mole fraction and growth temperature.[4,7]

IV. CONCLUSIONS

Off-axis electron holography has been used to map the electrostatic potential profile across the *p-n* junction of an InGaAs quantum well LED with nanometer-scale resolution. Comparisons of the measured and simulated *p-n* potential profiles indicated carrier-trap concentrations of 6×10^{16} cm^{-3} in the graded AlGaAs barriers of the LED away from the InGaAs regions.

Overall, this study has confirmed the ability of electron holography to provide useful quantitative information about dopant distributions across graded heterojunctions. Moreover, electron holography measurements combined with straightforward modeling should provide growers with a powerful tool for monitoring the effect of deep-level impurity traps, such as oxygen, on the doping efficiency in complex heterostructures.

ACKNOWLEDGMENTS

This work was partially supported by the Department of Energy Grant No. DE-FG02-04ER46168. We acknowledge use of facilities within the John M. Cowley Center for High Resolution Electron Microscopy at Arizona State University.

[1] H. Kroemer, Proc. IRE **45**, 1535 (1957).
[2] Z. I. Alferov and R. F. Kazarinov, Patent Application No. 950840 30 March, 1963.
[3] C. L. Allyn, A. C. Gossard, and W. Wiegmann, Appl. Phys. Lett. **36**, 373 (1980).
[4] M. E. Daniels, P. J. Bishop, K. D. Jensen, B. K. Ridley, D. A. Ritchie, M. Grimshaw, E. H. Linfield, G. A. C. Jones, and G. W. Smith, J. Appl. Phys. **74**, 5606 (1993).
[5] K. Akimoto, M. Kamada, K. Taira, M. Arai, and N. Watanabe, J. Appl. Phys. **59**, 2833 (1986).
[6] Y. Mihashi, M. Miyashita, N. Kaneno, M. Tsugami, N. Fujii, S. Takamiya, and S. Mitsui, J. Cryst. Growth **141**, 22 (1994).
[7] K. Yamanaka, S. Naritsuka, K. Kanamoto, M. Mihara, and M. Ishii, J. Appl. Phys. **61**, 5062 (1987).
[8] S. Naritsuka, O. Kobayashi, K. Mitsuda, and T. Nishinaga, J. Cryst. Growth **254**, 310 (2003).
[9] M. R. McCartney and D. J. Smith, Annu. Rev. Mater. Sci. **37**, 729 (2007).
[10] M. R. McCartney, D. J. Smith, R. Hull, J. C. Bean, E. Voelkl, and B. Frost, Appl. Phys. Lett. **65**, 2603 (1994).
[11] H. Lichte, P. Formanek, A. Lenk, M. Linck, C. Matzeck, M. Lehmann, and P. Simon, Annu. Rev. Mater. Sci. **37**, 539 (2007).
[12] M. A. Gribelyuk, M. R. McCartney, J. Li, C. S. Murthy, P. Ronsheim, B. Doris, J. S. McMurray, S. Hegde, and D. J. Smith, Phys. Rev. Lett. **89**, 025502 (2002).
[13] M. G. Han, P. Fejes, Q. Xie, S. Bagchi, B. Taylor, J. Conner, and M. R. McCartney, IEEE Trans. Electron Devices **54**, 3336 (2007).
[14] N. Ikarashi, T. Ikezawa, K. Uejima, T. Fukai, M. Miyamura, A. Toda, and M. Hane, J. Appl. Phys. **103**, 114514 (2008).
[15] A. T. Tilke, A. Lenk, U. Muhle, C. Wagner, C. Dahl, and H. Lichte, IEEE Trans. Electron Devices **52**, 1067 (2005).
[16] Z. H. Wu, A. M. Fischer, F. A. Ponce, W. Lee, J. H. Ryou, J. Limb, D. Yoo, and R. D. Dupuis, Appl. Phys. Lett. **91**, 041915 (2007).
[17] M. G. Han, J. Li, Q. Xie, P. Fejes, J. Conner, B. Taylor, and M. R. McCartney, Microsc. Microanal. **12**, 295 (2006).
[18] S. Chung, D. J. Smith, and M. R. McCartney, Microsc. Microanal. **13**, 329 (2007).
[19] W. D. Rau, P. Schwander, F. H. Baumann, W. Höppner, and A. Ourmazd, Phys. Rev. Lett. **82**, 2614 (1999).
[20] D. Cooper, A. C. Twitchett, P. K. Somodi, P. A. Midgley, R. E. Dunin-Borkowski, I. Farrer, and D. A. Ritchie, Appl. Phys. Lett. **88**, 063510 (2006).
[21] A. Lenk, H. Lichte, and U. Muehle, J. Electron Microsc. **54**, 351 (2005).
[22] M. R. McCartney, D. J. Smith, R. F. C. Farrow, and R. F. Marks, J. Appl. Phys. **82**, 2461 (1997).
[23] M. Gajdardziska-Josifovska, M. R. McCartney, W. J. de Ruijter, D. J. Smith, J. K. Weiss, and J. M. Zuo, Ultramicroscopy **50**, 285 (1993).
[24] W. J. de Ruijter and J. K. Weiss, Ultramicroscopy **50**, 269 (1993).
[25] S. Hillyard and J. Silcox, Ultramicroscopy **58**, 6 (1995).
[26] M. R. McCartney and M. Gajdardziska-Josifovska, Ultramicroscopy **53**, 283 (1994).
[27] J. Li, M. R. McCartney, and D. J. Smith, Ultramicroscopy **94**, 149 (2003).
[28] G. Snider, 1D Poisson program, available at http://www.nd.edu/~gsnider/.
[29] S. Chung, S. R. Johnson, Y.-H. Zhang, D. J. Smith, and M. R. McCartney, IEEE Trans. Electron Devices **56**, 1919 (2009).
[30] S. R. Johnson, Y. G. Sadofyev, D. Ding, Y. Cao, S. A. Chaparro, K. Franzreb, and Y.-H. Zhang, J. Vac. Sci. Technol. B **22**, 1436 (2004) (Be doping efficiencies for lower Al content AlGaAs do not appear to be available in the literature).